



Large out-of-plane piezoelectric effect in a Janus ferromagnetic semiconductor monolayer of CrOFBr

Qiuyue Ma, Guochun Yang, Busheng Wang , and Yong Liu ^{*}

State Key Laboratory of Metastable Materials Science and Technology & Key Laboratory for Microstructural Material Physics of Hebei Province, School of Science, *Yanshan University*, Qinhuangdao 066004, China



(Received 28 June 2024; revised 30 July 2024; accepted 7 August 2024; published 26 August 2024)

The exploitation of piezoelectric ferromagnetism in two-dimensional (2D) materials with large out-of-plane piezoelectric response is motivated not only by technological applications but also scientific interest. In this study, the CrONM monolayer family ($N = \text{F, Cl}; M = \text{Br, Cl}$) was investigated using first-principles calculations, revealing that the Janus CrOFBr monolayer exhibits intrinsic ferromagnetic semiconductor behavior along with a significant out-of-plane piezoelectric effect. The calculated out-of-plane piezoelectric strain coefficients d_{31} and d_{32} are up to 1.21 and 0.63 pm/V, respectively. These values are greater than those of the majority of 2D materials. Furthermore, our findings demonstrate that applying tensile strain can enhance the out-of-plane piezoelectric response, leading to a respective 27% and 67% augmentation in the piezoelectric strain coefficients d_{31} and d_{32} compared to the unstrained configurations. This discovery holds great potential for propelling the field of nanoelectronics forward and facilitating the development of multifunctional semiconductor spintronic applications. Finally, by comparing d_{31} and d_{32} of the CrONM monolayer family ($N = \text{F, Cl}; M = \text{Br, Cl}$), we find that the magnitudes of d_{31} and d_{32} are correlated with the electronegativity difference ratio. These findings provide valuable insights for the design of 2D piezoelectric materials with enhanced vertical piezoelectric responses.

DOI: [10.1103/PhysRevB.110.064430](https://doi.org/10.1103/PhysRevB.110.064430)

I. INTRODUCTION

Since the discovery of graphene in 2004, two-dimensional (2D) materials have garnered significant attention theoretically and experimentally [1–4]. Their intrinsic conductivity and tunable properties make them highly promising prospects for the advancement of next-generation devices and technologies. Magnetically ordered 2D materials bring numerous possibilities for new device concepts and physical phenomena, especially 2D magnetic semiconductors, offering unique opportunities for the exploration of low-dimensional magnetism. The 2D ferromagnetic (FM) semiconductors are considered highly promising candidates for nanospintronic devices, combining the advantages of 2D, magnetism, and semiconductivity properties. Unfortunately, 2D intrinsic FM semiconductors are rare due to the incompatibility between semiconductivity and magnetism. Until 2017, the advent of two 2D intrinsic FM semiconductors ($\text{Cr}_2\text{Ge}_2\text{Te}_6$ [5] and CrI_3 [6]) opened up opportunities for achieving scalable spintronic architecture.

2D FM materials that incorporate other appealing electronic characteristics, such as topology, valley properties, and piezoelectricity, can enhance device capabilities and pave the way for innovative nanoscale devices. Topological features have been identified in 2D FM materials like Fe_2IX ($X = \text{Cl}$ and Br) [7], FeX_2 ($X = \text{Cl, Br, I}$) [8], and VSiGeN_4 [9]. Valley properties have been observed in 2D FM

$1T - \text{CrXY}$ ($X = \text{S, Se, Te}, Y = \text{F, Cl, Br, I}$) [10], VGe_2P_4 [11]. In recent years, the piezoelectric properties of semiconductors have also attracted extensive research interest [12–15]. The piezoelectric effect is the phenomenon of electric dipole moments induced in noncentrosymmetric materials by mechanical stress [16]. Reports on 2D piezoelectric materials are increasingly emerging, both theoretically and experimentally. A number of 2D multifunctional piezoelectric materials have been predicted by first-principles calculations, including Janus group-III chalcogenide [17], group IV monochalcogenides [18], and transition-metal dichalcogenides (TMD) [19]. Experimentally, 2H-MoS_2 has emerged as a prototypical 2D piezoelectric material, and its discovery has significantly advanced the understanding and exploration of piezoelectric properties in 2D materials [20]. By integrating piezoelectricity and magnetism within a 2D material, known as 2D piezoelectric ferromagnetism (PFM), significant advancements have been achieved in 2D vanadium dihalides, such as VS_2 , VSe_2 , and Janus VSSe , which not only exhibit magnetic semiconductor behavior but also demonstrate remarkable piezoelectric response [21].

In recent years, 2D Janus materials have been introduced as a promising new class of materials. Due to the breaking of inversion and mirror symmetry, Janus materials exhibit many fascinating physical properties. Out-of-plane asymmetry leads to Rashba spin splitting in Janus $\text{Ga}_2\text{Ge}_2\text{XY}$ ($X, Y = \text{S, Se, and Te}$) monolayers [22]. Additionally, Janus ZnAXY ($A = \text{Si, Ge, Sn}$ and $X, Y = \text{S, Se, Te}$) monolayers also exhibit the Rashba effect. Notably, the Rashba parameter for Janus ZnGeSTe is the highest (~ 1.79 eV Å), significantly

^{*}Contact author: yongliu@ysu.edu.cn

higher than the largest Rashba parameters reported for Janus TMDs [23]. Some Janus structures exhibit high electron mobility, such as Janus Bi_2Se_3 monolayer ($5442 \text{ cm}^2 \text{ V}^{-1} \text{ s}^{-1}$) [24], $\gamma - \text{Ge}_2\text{STe}$ ($3220 \text{ cm}^2 \text{ V}^{-1} \text{ s}^{-1}$), and $\gamma - \text{Ge}_2\text{SeTe}$ ($8330 \text{ cm}^2 \text{ V}^{-1} \text{ s}^{-1}$) monolayers [25], demonstrating that they are very suitable for applications in high-speed nanoelectronic devices. The Janus BInSe_2 monolayer is a novel zero-gap ferroelectric material with quadratic energy dispersion. It exhibits high spontaneous polarization and demonstrates high absorption for light across a broad spectrum, ranging from the infrared to the ultraviolet [26]. Recently, a class of magnets called altermagnets, which exhibit zero net magnetization and spin-split electronic bands, has been gaining increasing attention in the field of spintronics [27,28]. The broken out-of-plane symmetry in the Janus altermagnets induces many intriguing physical properties [29]. The Janus altermagnetic V_2SeTeO monolayer exhibits a novel “multipiezo” effect, combining piezoelectricity, piezovolley, and piezomagnetism, making it a promising material for potential applications in nanoelectronics, optoelectronics, spintronics, and valleytronics [30]. Another Janus altermagnet, Cr_2SO monolayer, exhibits spin-valley polarization and demonstrates large out-of-plane piezoelectricity, making it highly desirable for ultrathin multifunctional device applications [31]. Furthermore, the Janus monolayers can switch between different spin-polarized states under varying gate voltages [32]. Biaxial strain and hole/electron doping can tune the electronic and magnetic properties of Janus structures [33,34]. These tunable physical properties enrich the diversity of Janus structures, making them promising candidates for spintronic device applications.

In 2D materials, centrosymmetric structures inherently lack intrinsic piezoelectricity, thus requiring the exploration of different approaches to elicit piezoelectric responses. The construction of a Janus structure is a new method that breaks the symmetry. The broken out-of-plane symmetry in these materials allows for the observation of out-of-plane piezoelectricity, offering the potential to identify materials with large out-of-plane piezoelectric response. Specifically, in Janus MXY materials with M sandwiched between X and Y , the different electronegativities of X and Y elements result in an obvious spontaneous polarization [19]. Thus, the Janus method provides a pathway to explore piezoelectric responses in 2D materials, and several related studies have already been conducted. Additionally, Janus MXY monolayers such as MoSSe have been successfully synthesized, indicating the potential for future applications [35]. On the other hand, the strain-tuned piezoelectric response of MoS_2 [36] and Janus TMD monolayer [37] has demonstrated that strain engineering provides an alternative solution for finding a significant out-of-plane piezoelectric response. So far, great advances have been made in 2D piezoelectric materials. However, there is a main issue of 2D piezoelectric materials, which is that the out-of-plane piezoelectricity in known 2D materials is absent or weak. For example, the monolayer of InCrTe_2 exhibits significant FM coupling and in-plane magnetic anisotropy. However, it has a weak out-of-plane piezoelectricity ($d_{31} = 0.39 \text{ pm/V}$). The strong out-of-plane piezoelectric effect and its inverse effect are highly desirable for piezoelectric devices, which is compatible with the bottom/top gate technologies. Therefore, it is necessary to find further 2D magnetic

materials with large out-of-plane piezoelectric properties for experimental studies and possible device applications.

Considering the charming piezoelectric nature of the Janus structure, in this work, we constructed the Janus CrOFBr monolayer structure, which can be obtained by replacing the F layer in the CrOF monolayer with Br atoms. Our calculations show that the Janus CrOFBr monolayer is dynamically, thermally, and mechanically stable. It is found that the Janus CrOFBr monolayer is a large gap intrinsic FM semiconductor. As a result of the broken horizontal mirror symmetry, the Janus CrOFBr monolayer possesses only out-of-plane piezoelectric response. The predicted out-of-plane piezoelectric coefficients d_{31} and d_{32} are 1.21 and 0.63 pm/V, respectively, which are higher than those of many 2D materials. Similar to Janus CrOFBr monolayer, the Janus CrOCIBr and CrOFCl monolayers are also intrinsic FM semiconductors with large out-of-plane piezoelectric response. Moreover, we investigate the biaxial strain effects on the physical properties of the Janus CrOFBr monolayer. The findings suggest that the application of biaxial strain does not induce phase transition. Additionally, it is found that tensile strain can improve d_{31} and d_{32} . The Janus CrOFBr monolayer may be a promising candidate for applications in spin electronic and piezoelectric devices.

II. METHODS

The first-principles calculations are performed using the projector augmented wave (PAW) method within density functional theory (DFT) [38,39] as implemented in the plane-wave code Vienna ab initio Simulation Package (VASP) [40–42]. The exchange and correlation effects are tackled by the generalized gradient approximation (GGA) formulation of Perdew-Burke-Ernzerhof (PBE) [43]. To account for the on-site Coulomb correlation of Cr-3d electrons, the GGA+ U scheme ($U = 7.0 \text{ eV}$) is employed for the Cr-3d electron [44,45], which has been tested in previous works [46,47]. The k -point grids of $15 \times 13 \times 1$ are employed to sample the Brillouin zone for the unit cell. The plane-wave cutoff energy of 500 eV, the total energy convergence criterion of 10^{-6} eV , and force convergence criteria of less than 0.01 eV/\AA on each atom are used to attain reliable results. A vacuum layer of at least 15 \AA along the z direction is added to avoid interactions between the neighboring images. The phonon spectrum with a $3 \times 3 \times 1$ supercell is calculated self-consistently with the use of the PHONOPY code [48]. *Ab initio* molecular-dynamics (AIMD) simulations in the canonical (NVT) ensemble are performed for 3000 fs at 300 K with a Nosé-Hoover thermostat [49]. The elastic stiffness tensor C_{ij} and piezoelectric stress tensor e_{ij} are calculated by using the strain-stress relationship (SSR) and density functional perturbation theory (DFPT) method [50]. The 2D elastic coefficients C_{ij}^{2D} and piezoelectric stress coefficients e_{ij}^{2D} have been renormalized by $C_{ij}^{2D} = Lz C_{ij}^{3D}$ and $e_{ij}^{2D} = Lz e_{ij}^{3D}$, where Lz is the length of unit cell along the z direction.

III. RESULTS AND DISCUSSION

The top and side views of the Janus CrOFBr monolayer are shown in Figs. 1(a)–1(c). It consists of a F-CrO-Br sandwich layer, which can be built by replacing one of two F layers

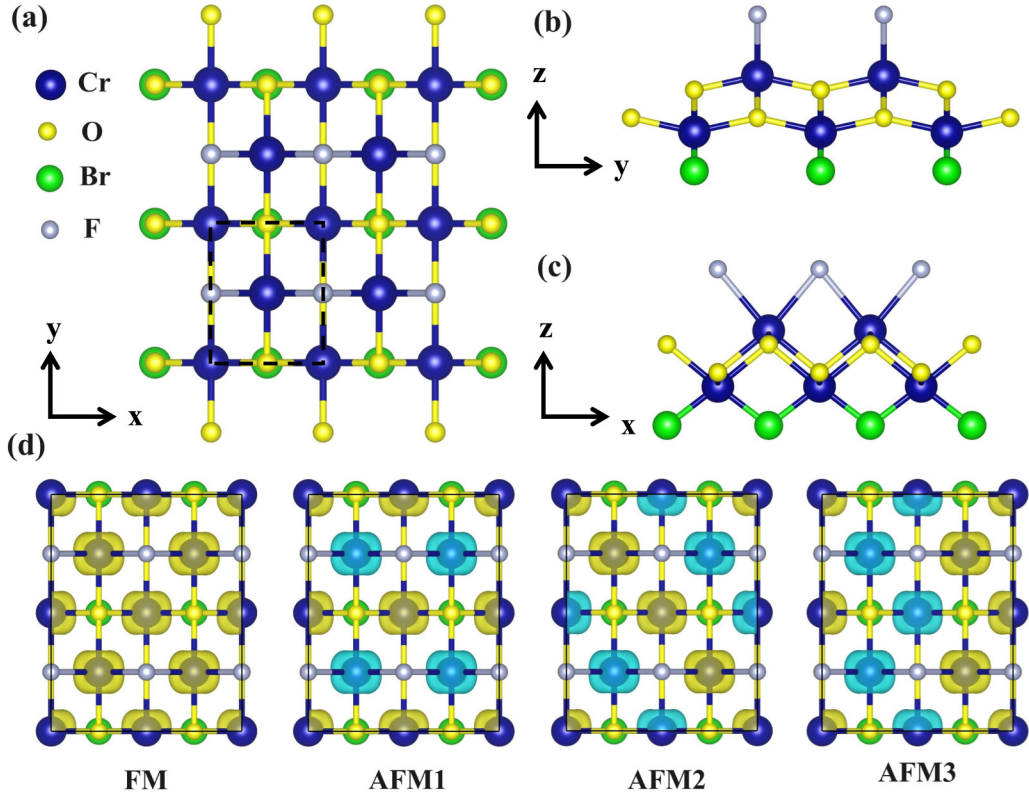


FIG. 1. (a) Top and (b), (c) side views of the Janus CrOFBr monolayer. (The area marked by a black dotted line is the corresponding primitive cell.) (d) The spatial distribution of spin-polarized electron density for the Janus CrOFBr monolayer in one ferromagnetic configuration and three antiferromagnetic configurations.

with Br atoms in a CrOF monolayer [51]. This gives rise to the formation of a typical Janus structure. The Janus CrOFBr monolayer has strongly distorted octahedron units. Each Cr atom is sixfold-coordinated with one F, one Br, and four O atoms. The presence of broken vertical mirror symmetry in the CrOFBr monolayer leads to its space group being $Pmm2$ (no. 25), which is lower in symmetry compared to the $Pmmn$ (no. 59) space group of the CrOF monolayer. For the CrOFBr monolayer, the disparity in atomic size and electronegativity between F and Br atoms leads to unequal bonding lengths and charge distributions in the Cr-F and Cr-Br bonds. This discrepancy generates an out-of-plane piezoelectric response and induces an electrostatic potential gradient. The optimized lattice parameters a and b are 3.202 and 3.977 Å, respectively. The bond lengths Cr-O, Cr-F, and Cr-Br of the Janus CrOFBr monolayer are found to be 2.04, 2.02, and 2.51 Å. To investigate the chemical bonding information of the Janus CrOFBr monolayer, we have calculated the crystal orbital Hamilton population (COHP). Figure S1 of the Supplemental Material shows the negative COHP curves for the CrOFBr monolayer [52]. The results indicate that the Cr- X ($X = O, Br, F$) bonds exhibit mainly bonding interactions above the Fermi level, while both bonding and antibonding interactions are present below the Fermi level. In addition, we calculated the negative integration of orbital Hamilton populations (-ICOHP) to reflect the bonding strength between atoms. Due to the relatively large distance between Cr atoms (3.10 Å), the -ICOHP between Cr atoms is much smaller compared to Cr-O, Cr-F, and Cr-Br. The -ICOHP values for Cr-O1, Cr-O2, Cr-F, and

Cr-Br are 1.11, 1.79, 1.23, and 1.19, respectively. It is evident that the bonding strength between Cr and O2 atoms is the strongest, and the -ICOHP values for Cr- X bonds are greater than those of some other 2D materials, indicating that CrOFBr possesses relatively good stability. Similarly, Janus CrOFCl and CrOCIBr monolayers can also be constructed from CrOF. Accordingly, the optimized lattice constants a , b , and bond lengths are summarized in Table I. As illustrated in Fig. 1(d), we considered the FM and three antiferromagnetic (AFM) configurations for the supercells of $2 \times 2 \times 1$ to determine the preferred magnetic ground state for Janus CrOFBr monolayer. Then, we performed spin-polarized DFT calculations. The energies of different magnetic configurations (FM, AFM1, AFM2, and AFM3) are detailed in Table SI of the Supplemental Material [52]. The positive energy differences confirm that the FM configuration is the ground state for the Janus CrOFBr monolayer. Meanwhile, we found that the ground states of the Janus CrOFCl, CrOFBr monolayers are also FM. Our analysis of the spatial distribution of the spin-polarized

TABLE I. Lattice constants a and b (Å), bond lengths (Å), and band gap (eV) of Janus CrOFCl, CrOFBr, and CrOCIBr monolayers.

	a	b	L_{Cr-O}	L_{Cr-N}	L_{Cr-M}	gap
CrOFCl	3.16	3.97	2.05	2.00	2.35	2.72
CrOFBr	3.20	3.98	2.04	2.02	2.51	1.67
CrOCIBr	3.31	3.98	2.08	2.39	2.52	1.78

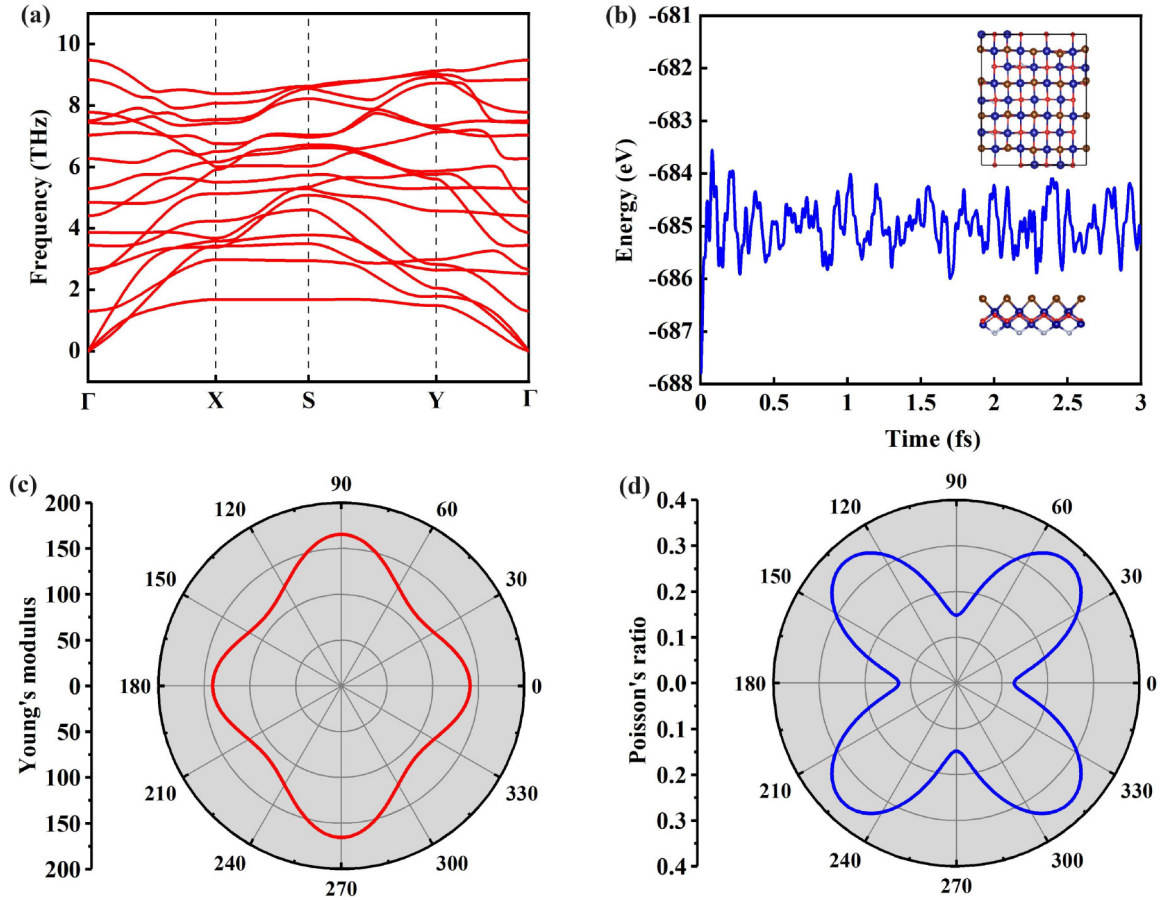


FIG. 2. Determination of the stability for Janus CrOFBr monolayer. (a) The phonon spectra, (b) total energy fluctuations with respect to AIMD simulation at 300 K, the angular dependence of (c) Young's modulus, and (d) Poisson's ratio.

electron density reveals that its large FM localized magnetic moment ($6\mu_B$ per unit cell) is primarily contributed by Cr atoms, with each Cr atom contributing approximately $3.2\mu_B$.

To verify the dynamical stability of the Janus CrOFBr monolayer, the phonon spectrum was calculated. As shown in Fig. 2(a), the absence of imaginary-frequency modes in the phonon band dispersion suggests the Janus CrOFBr monolayer meets dynamic stability. The phonon spectrum presented in Fig. S2 [52] proves that Janus CrOFCl and CrOCIBr monolayers are also dynamically stable. To further confirm the thermal stability, we performed AIMD simulations of the $4 \times 4 \times 1$ supercells for 3000 fs at 300 K. Figure 2(b) shows the total energy fluctuations of the Janus CrOFBr monolayer as a function of the simulation time. The calculated results indicate no significant structural disturbance as the total energy fluctuates, confirming the thermodynamic stability of the Janus CrOFBr monolayer at room temperature. It is crucial to examine the practical applicability of the Janus CrOFBr monolayer. Therefore, we employed the SSR method to calculate the elastic stiffness tensor, allowing for the evaluation of the material's mechanical properties. The 2D elastic stiffness tensor (Voigt notation) with point group $Pmm2$ can be reduced to

$$\begin{pmatrix} C_{11} & C_{12} & 0 \\ C_{12} & C_{22} & 0 \\ 0 & 0 & C_{66} \end{pmatrix}. \quad (1)$$

Our calculated elastic stiffness tensors C_{11} , C_{12} , C_{22} , and C_{66} are 143.31, 21.26, 168.62, and 41.51 N/m, respectively, which satisfy the Born-Huang criteria of mechanical stability ($C_{11} > 0$, $C_{22} > 0$, $C_{66} > 0$, $C_{11} - C_{12} > 0$), thereby indicating the Janus CrOFBr monolayer is mechanically stable. Young's modulus $Y_{2D}(\theta)$ and Poisson's ratios $\nu_{2D}(\theta)$ can be calculated on the basis of the elastic stiffness tensors C_{ij} . The in-plane $Y_{2D}(\theta)$ and $\nu_{2D}(\theta)$ can be calculated by the following two formulas [53,54]:

$$Y_{2D}(\theta) = \frac{C_{11}C_{22} - C_{12}^2}{C_{11}m^4 + C_{22}n^4 + (B - 2C_{12})m^2n^2}, \quad (2)$$

$$\nu_{2D}(\theta) = \frac{(C_{11} + C_{22} - B)m^2n^2 - C_{12}(m^4 + n^4)}{C_{11}m^4 + C_{22}n^4 + (B - 2C_{12})m^2n^2}, \quad (3)$$

where θ is the angle of the direction, with the x direction as 0° and the y direction as 90° , $m = \sin(\theta)$, $n = \cos(\theta)$, and $B = (C_{11}C_{22} - C_{12}^2)/C_{66}$. The $Y_{2D}(\theta)$ and $\nu_{2D}(\theta)$ as a function of the angle θ are plotted in Figs. 2(c) and 2(d). Because the CrOFBr monolayer is an asymmetric structure, the Y_{2D} and ν_{2D} of Janus CrOFBr monolayer show anisotropy along the (100) and (010) directions. The Y_{2D} and ν_{2D} are 140.63/165.47 and 0.126/0.148 N/m along the (100)/(010) direction. The softest direction is along the (110) direction, with its Y_{2D} of

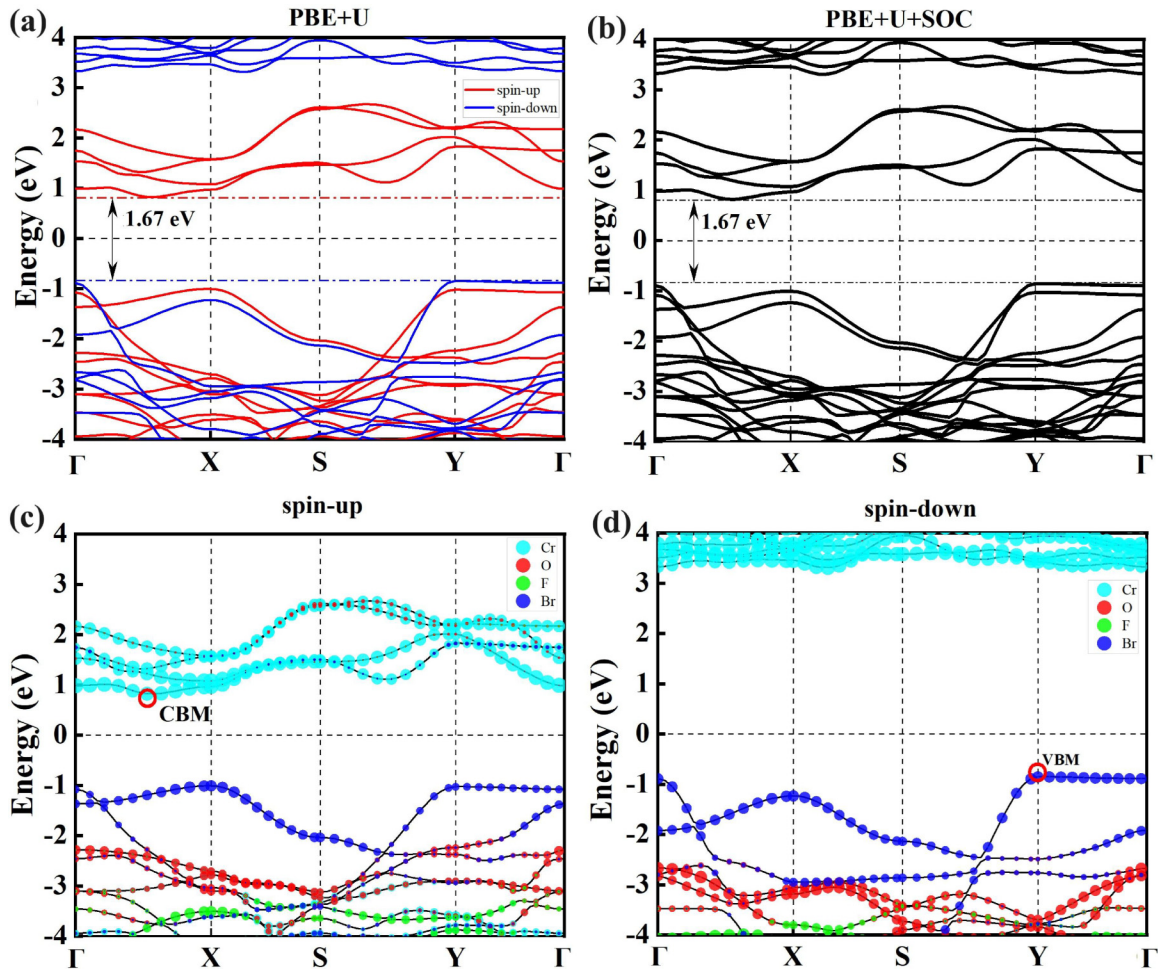


FIG. 3. The electronic band structures of Janus CrOFBr monolayer calculated by (a) PBE + U , and (b) PBE + U + SOC methods. The projected electronic band structures for (c) spin-up and (d) spin-down states of CrOFBr monolayer.

112.83 N/m, and the maximum value of ν_{2D} is 0.359 along the (110) direction.

As shown in Figs. 3(a) and 3(b), the band structures for Janus CrOFBr monolayer in the ground magnetic state were investigated by using PBE + U and PBE + U + spin-orbit coupling (SOC) methods. The PBE + U result shows that the Janus CrOFBr monolayer is an indirect-gap semiconductor with a large band gap of 1.67 eV. The Janus CrOFBr monolayer exhibits a significant discrepancy of 2.49 eV between the conduction-band minimum of its two spin channels, making it a promising candidate for spin-polarized carrier injection and detection applications. Additionally, we employed the PBE + U + SOC method to calculate the band structure of the Janus CrOFBr monolayer. The results indicate that there is no significant difference in the electronic band structure (with a gap of 1.67 eV) after considering the SOC. This suggests that the electronic structure of the Janus CrOFBr monolayer has a negligible effect induced by SOC. To further explore the electronic properties of Janus CrOFBr monolayer, the projected electronic band structures are shown in Figs. 3(c) and 3(d). The valence-band maximum (VBM) of CrOFBr is located at point Y and the conduction-band minimum (CBM) is at one point along the $\Gamma - X$ path, respectively. For the

purpose of comparing the electronic structural characteristics of CrOFBr with two other compounds, we have included the band structures of CrOFCl and CrOClBr in Fig. S3 [52]. It is evident that the band structures of all three compounds exhibit a remarkable similarity. Notably, CrOFCl stands out with the largest band gap, measuring 2.71 eV.

The magnetic anisotropy energy (MAE) is one of the most important properties of 2D magnetic materials. The angular dependence of the MAE of the CrOFBr monolayer in the $x - y$ plane is shown in Fig. 4(a). The relative energy of M_C [001] is set to zero. Consequently, the easy and hard magnetization axes correspond to the z -axis and y -axis, respectively, and the MAE of the CrOFBr monolayer reaches 0.21 meV per unit cell. SOC is a crucial interaction in magnetic materials that can significantly influence the MAE. Due to the strong spin-orbit coupling in heavier atoms, the MAE in CrOFBr monolayer is primarily contributed by the F atom. Figure S4 [52] shows the MAE contributed by the F- p orbital projection. The results indicate that the SOC interactions between the p_x and p_z orbitals of the F atom primarily contribute to the out-of-plane MAE of the Janus CrOFBr monolayer. To evaluate the potential practical applications of Janus CrOFBr monolayer in spintronic devices, we conducted additional Monte Carlo

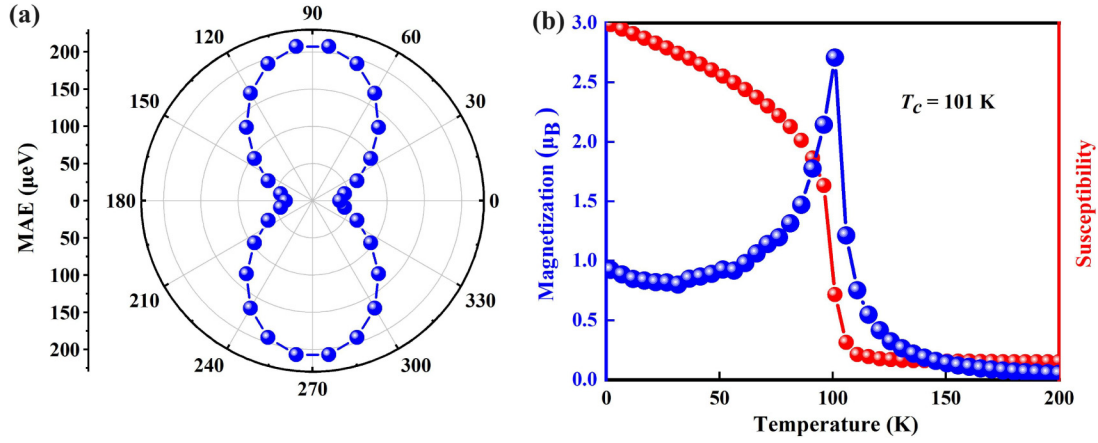


FIG. 4. (a) Angular dependence of MAE of the Janus CrOFBr monolayer in the $x - y$ plane. The relative energy of Mc (001) is assigned as zero, representing the easy magnetic axis. (b) Magnetic moment and specific heat with respect to temperature for Janus CrOFBr monolayer.

(MC) simulations with the Heisenberg model to calculate the variation trend of magnetism with temperature. The spin Hamiltonian can be considered as

$$H = - \sum_{(i,j)} J_1 S_i S_j - \sum_{(k,l)} J_2 S_k S_l - \sum_{(m,n)} J_3 S_m S_n. \quad (4)$$

Here, the value of S is $3/2$, which represents the spin of Cr atom. J_1 , J_2 , and J_3 represent the first-nearest, second-nearest, and third-nearest magnetic coupling parameters, respectively. Using the Heisenberg model Hamiltonian, the following energy equations can be written for different magnetic orders:

$$E(\text{FM}) = E_0 - (4J_1 + 2J_2 + 2J_3)S^2, \quad (5)$$

$$E(\text{AFM1}) = E_0 - (-4J_1 + 2J_2 + 2J_3)S^2, \quad (6)$$

$$E(\text{AFM2}) = E_0 - (-2J_2 - 2J_3)S^2, \quad (7)$$

$$E(\text{AFM3}) = E_0 - (-2J_2 + 2J_3)S^2. \quad (8)$$

The three calculated exchange coupling parameters J_1 , J_2 , and J_3 are 1.52, 0.86, and 2.73 meV, respectively. Due to the positive values of J , the FM configuration is the magnetic configuration of Janus CrOFBr monolayer. The variation of the magnetic moment and the susceptibility as a function of temperature that was considered through the MC simulation is illustrated in Fig. 4(b). Corresponding to the peak position of the specific heat (C_V), which is defined by $C_V = (\langle E^2 \rangle - \langle E \rangle^2) / K_B T^2$, and the local magnetic moments on Cr atoms beginning to drop sharply, the calculated T_c of Janus CrOFBr monolayer is 101 K, which is higher than the T_c of $\text{Cr}_2\text{Ge}_2\text{Te}_6$ bilayer (30 K) [5] and CrI_3 monolayer (45 K) [6]. Furthermore, the Janus CrOFCl and CrOCIBr monolayers also possess out-of-plane magnetic anisotropy based on MAE, and their T_c values reach 110 and 104 K, respectively.

The piezoelectric effect refers to the phenomenon in non-centrosymmetric materials where the application of strain or stress causes a change in charge distribution, leading to electric dipole moments and producing electricity. This phenomenon arises from the lack of inversion symmetry in the crystal structure of piezoelectric materials. The CrOFBr monolayer is a noncentrosymmetric structure, which means that it possesses a piezoelectric effect. Simultaneously, we

calculated the average potential energy distribution along the z -axis, as depicted in Fig. S5 [52]. The results indicate a significant potential difference between the upper and lower surfaces of the 2D structure. Using the formula for the built-in electric field and considering the interatomic distance, we determined the intrinsic electric field strength of the Janus CrOFBr monolayer to be $1.03 \text{ eV}/\text{\AA}$. This value is notably high compared to those reported for other 2D piezoelectric materials, further suggesting the potential piezoelectricity in the Janus CrOFBr monolayer. Next, we specifically investigate the piezoelectric properties of the Janus CrOFBr monolayer. The piezoelectric effects of a material can be described by third-rank piezoelectric tensors e_{ijk} and piezoelectric strains d_{ijk} , where the relaxed e_{ijk} and d_{ijk} are the sum of contributions from both ions and electrons:

$$e_{ijk} = \frac{\partial P_i}{\partial \varepsilon_{jk}} = e_{ijk}^{\text{elec}} + e_{ijk}^{\text{ion}} \quad (9)$$

and

$$d_{ijk} = \frac{\partial P_i}{\partial \sigma_{jk}} = d_{ijk}^{\text{elec}} + d_{ijk}^{\text{ion}}. \quad (10)$$

The relationship between e_{ijk} and d_{ijk} can be expressed as follows:

$$e_{ijk} = \frac{\partial P_i}{\partial \varepsilon_{jk}} = \frac{\partial P_i}{\partial \sigma_{mn}} \frac{\partial \sigma_{mn}}{\partial \varepsilon_{jk}} = d_{imn} C_{mnjk}, \quad (11)$$

where P_i , ε_{jk} , and σ_{jk} represent the piezoelectric polarizations, strains, and stresses, respectively. C_{mnjk} is an elastic stiffness tensor. For 2D materials, only the in-plane strain and stress are taken into account [55–59]. Using Voigt notation, the piezoelectric stress and piezoelectric strain tensors with $Pmm2$ point group symmetry can be expressed as

$$\begin{pmatrix} 0 & 0 & 0 \\ 0 & 0 & 0 \\ e_{31} & e_{32} & 0 \end{pmatrix}, \quad (12)$$

$$\begin{pmatrix} 0 & 0 & 0 \\ 0 & 0 & 0 \\ d_{31} & d_{32} & 0 \end{pmatrix}. \quad (13)$$

TABLE II. Elastic constants C_{ij} (N/m), and the piezoelectric coefficients e_{ij} (10^{-10} C/m) and d_{ij} (pm/V) for Janus CrOCIBr, CrOFCl, and CrOFBr monolayers.

	C_{11}	C_{12}	C_{22}	e_{31}	e_{32}	d_{31}	d_{32}
CrOCIBr	121.94	20.78	159.88	0.61	0.38	0.47	0.18
CrOFCl	140.60	21.65	167.23	1.27	1.10	0.80	0.47
CrOFBr	143.31	21.26	168.62	1.87	1.38	1.21	0.63

When a uniaxial in-plane strain is imposed, the vertical piezoelectric polarization ($d_{31} \neq 0$ or $d_{32} \neq 0$) can be induced. However, by imposing biaxial in-plane strain, the superposed out-of-plane polarization will arise ($d_{31} \neq 0$ and $d_{32} \neq 0$). The d_{31} and d_{32} can be calculated by Eqs. (11)–(13):

$$d_{31} = \frac{e_{31}C_{22} - e_{32}C_{12}}{C_{11}C_{22} - C_{12}^2}, \quad (14)$$

$$d_{32} = \frac{e_{32}C_{11} - e_{31}C_{12}}{C_{11}C_{22} - C_{12}^2}. \quad (15)$$

The e_{31} and e_{32} of Janus CrOFBr monolayer can be directly calculated by DFPT. The calculated e_{31} (e_{32}) is 1.87×10^{-10} C/m (1.38×10^{-10} C/m) with the ionic part -0.40×10^{-10} C/m (-0.03×10^{-10} C/m) and the electronic part 2.27×10^{-10} C/m (1.35×10^{-10} C/m). The contributions from both electrons and ions to e_{31} and e_{32} have opposite signs, with the electronic contribution dominating the piezoelectricity. According to Eqs. (14) and (15), the calculated d_{31} and d_{32} are 1.21 and 0.63 pm/V, which are significantly larger than those of most known 2D materials, like Janus group-III materials (0.46 pm/V) [17], Janus transition-metal dichalcogenide (TMD) monolayers (0.03 pm/V) [19], Janus BiTeI/SbTeI monolayer (0.37–0.66 pm/V) [60], and oxygen functionalized MXenes (0.40–0.78 pm/V) [61]. The large out-of-plane piezoelectricity observed in the Janus CrOFBr monolayer provides broad prospects for the development and design of novel piezoelectric devices. Accordingly, we also calculated the piezoelectric properties of Janus CrOFCl and CrOCIBr monolayers. The piezoelectric stress coefficients (e_{31} and e_{32}), piezoelectric strain coefficients (d_{31} and d_{32}), and elastic tensors (C_{11} , C_{12} , and C_{22}) of Janus CrOCIBr, CrOFCl, and CrOFBr monolayers are plotted in Fig. 5, and the corresponding data are summarized in Table II. Research has shown that the variation trend of piezoelectricity follows the variation trend of the electronegativity difference ratio [22,62,63]. Next, we discuss the relationship between the electronegativity difference ratio and piezoelectricity in the CrONM ($N = \text{F,Cl}$; $M = \text{Br,Cl}$) system in detail. The electronegativity difference ratio can be obtained by the following formula [64]:

$$r_{\text{ed}} = \frac{|N_{\text{eln}} - Cr_{\text{eln}}|}{|M_{\text{eln}} - Cr_{\text{eln}}|}, \quad (16)$$

where N_{eln} , M_{eln} , and Cr_{eln} represent the electronegativities of F/Cl, Br/Cl, and Cr atoms, respectively. The calculated r_{ed} values for CrOCIBr, CrOFCl, and CrOFBr monolayers are 1.15, 1.54, and 1.78, respectively. As shown in Fig. S6 [52],

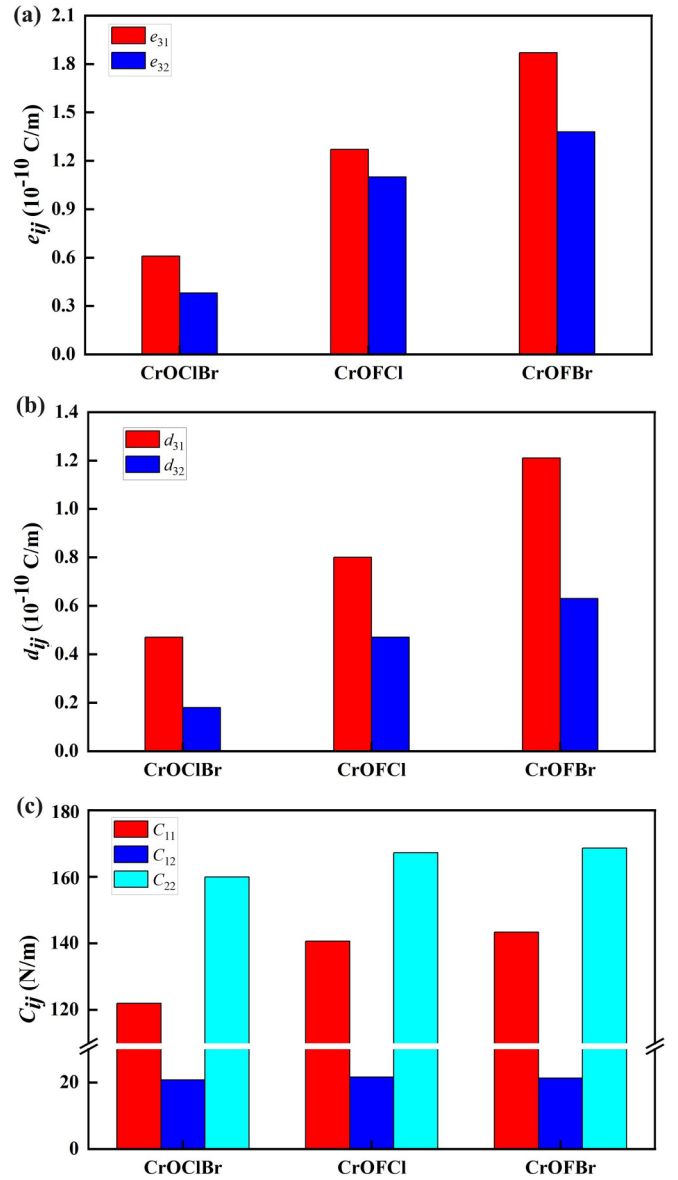


FIG. 5. (a) Piezoelectric stress coefficients e_{31} and e_{32} , (b) piezoelectric strain coefficients d_{31} and d_{32} , and (c) elastic tensors C_{11} , C_{12} , and C_{22} for Janus CrOCIBr, CrOFCl, and CrOFBr monolayers.

the results indicate that as the electronegativity difference ratio increases, the piezoelectric strain coefficient continuously increases. Consequently, we can conclude that a higher electronegativity difference ratio corresponds to a higher piezoelectricity. Greater electronegativity difference implies a larger amount of electron transfer and more asymmetric electron distribution, resulting in higher piezoelectricity. Thus, materials with a significant electronegativity difference ratio would be a potential way to find high piezoelectric materials.

Next, the influence of biaxial strain on the electronic structures and the piezoelectric properties of the Janus CrOFBr monolayer was investigated. Studies have demonstrated that strain engineering can effectively modulate the electronic structures and piezoelectric characteristics of 2D materials [34,37,65]. Here, a/a_0 is used to simulate the biaxial strain,

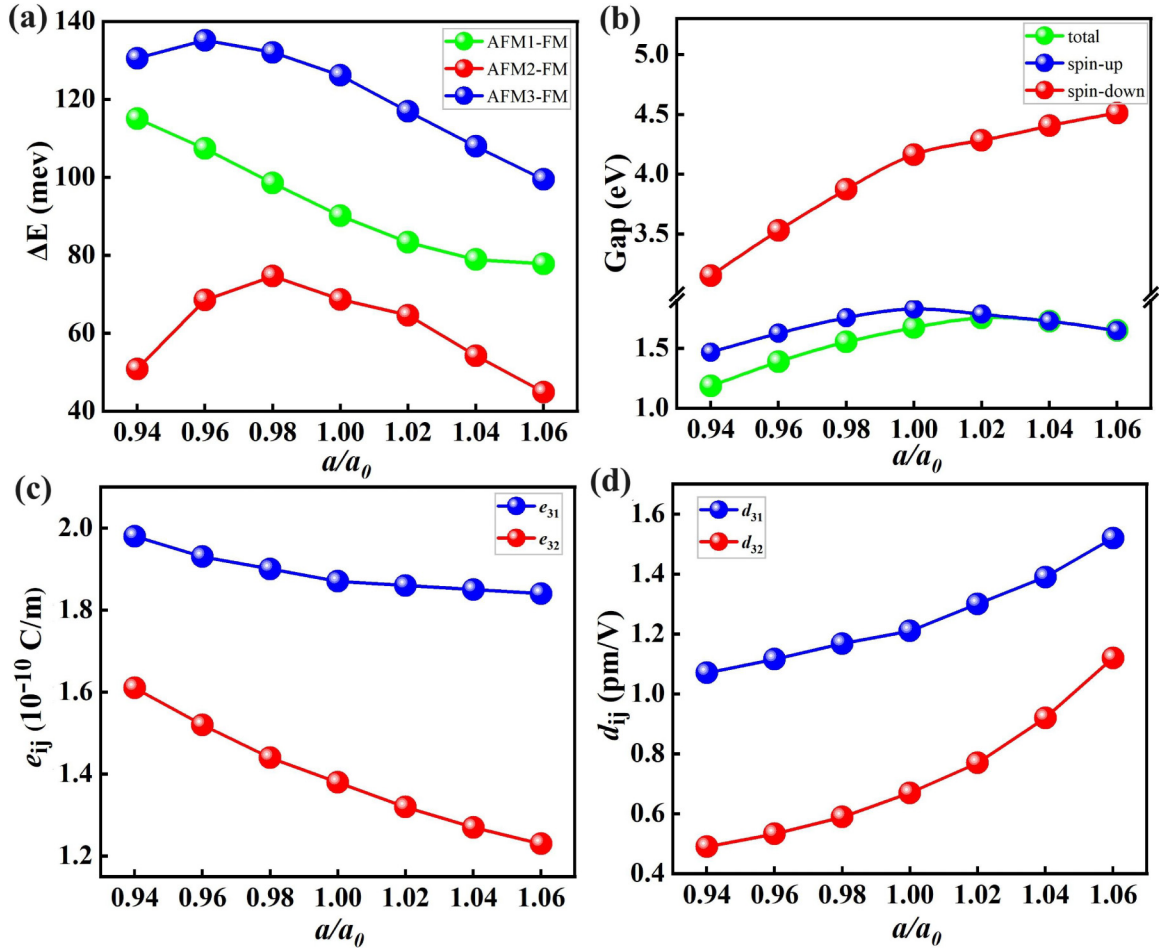


FIG. 6. For Janus CrOFBr monolayer, (a) the energy differences of AFM1, AFM2, and AFM3 with respect to FM state, (b) the spin-up gap, the spin-down gap, and the total gap, (c) piezoelectric stress coefficients, and (d) piezoelectric strain coefficients as a function of a/a_0 .

where a and a_0 represent the strained and unstrained lattice constants, respectively. We investigated the effects of a/a_0 ranging from 0.94 to 1.06 on the properties of the Janus CrOFBr monolayer. Figure 6(a) illustrates the variation of the energy differences between the FM and three AFM configurations as a function of a/a_0 , all of which exhibit positive values. This indicates that the FM state always corresponds to the ground state in the biaxial strain range of 0.94–1.06. The energy band structures of the Janus CrOFBr monolayer, with the a/a_0 ranging from 0.94 to 1.06, are depicted in Fig. S7 [52]. It indicates that the CrOFBr is always an indirect-band-gap semiconductor at different biaxial strains. At a/a_0 ranging from 0.94 to 1.06, the CBM is located at one point along the $\Gamma - X$ path. At a compressive strain, the VBM of the Janus CrOFBr monolayer is located at the Y point; however, the VBM moves from point Y to point X at $a/a_0 = 1.02$. The spin-up gap, the spin-down gap, and the total gap of Janus CrOFBr monolayer as a function of a/a_0 are plotted in Fig. 6(b). It is clearly seen that the a/a_0 ranging from 0.94 to 1.06 causes the conduction band and valence band of the spin-down channel to move away from the Fermi level, resulting in an increase in the spin-down gap. The total band gap undergoes an initial increase and then decreases within the biaxial strain range, reaching a maximum value of 1.76 eV at $a/a_0 = 1.02$. The results show that the spin-up and total gaps coincide at

a/a_0 of 1.02–1.06, which means that Janus CrOFBr monolayer exhibits half semiconductor character. Additionally, the piezoelectric stress coefficients (e_{31} and e_{32}) and piezoelectric strain coefficients (d_{31} and d_{32}) of Janus CrOFBr monolayer as a function of a/a_0 are shown in Fig. 6(a). It is found that compressive strain can enhance e_{31} (e_{32}), and at $a/a_0 = 0.94$, e_{31} (e_{32}) improves to 1.98 (1.61) pm/V from the unstrained value of 1.87 (1.38) pm/V. On the other hand, tensile strain can decrease e_{31} (e_{32}), and at $a/a_0 = 1.06$, e_{31} (e_{32}) reduces to 1.84 (1.23) pm/V. Both the d_{31} and d_{32} coefficients of the Janus CrOFBr monolayer exhibit an increase as the a/a_0 varies from 0.94 to 1.06. The values of d_{31} and d_{32} reach a maximum of 1.52 and 1.12 pm/V at $a/a_0 = 1.06$, which represents a 27% and 67% increase relative to the unstrained value. Meanwhile, we also calculated the effect of biaxial strain on the piezoelectric strain coefficients (d_{31} and d_{32}) of Janus CrOCIBr and CrOFCI monolayers, as shown in Fig. S8 [52]. It is clearly seen that the out-of-plane strain piezoelectric coefficients are also significantly enhanced as the a/a_0 increases. Figure S9 [52] illustrates the projected magnetic moment of the Cr atom and the out-of-plane piezoelectric coefficients (d_{31} and d_{32}) in the Janus CrOFBr monolayer under biaxial strain. We found that the influence of biaxial strain on both the magnetic moment of the Cr atom and the out-of-plane piezoelectric coefficients exhibits similar trends.

IV. CONCLUSION

In summary, we predicted that the Janus CrOFBr monolayer with space group $Pmm2$, characterized by outstanding dynamic, thermal, and mechanical stabilities, demonstrates intrinsic FM semiconductor behavior based on first-principles calculations. Due to structural symmetry breaking, the Janus CrOFBr monolayer only possesses out-of-plane piezoelectric response. The calculated out-of-plane piezoelectric coefficients d_{31} and d_{32} are 1.21 and 0.63 pm/V, respectively, significantly exceeding those found in the majority of known 2D materials. This significant out-of-plane piezoelectricity indicates that the monolayer has great potential for the operation and design of new piezoelectric devices. Additionally, the Janus CrOCIBr and CrOFCl monolayers are also promising intrinsic FM semiconductors with large out-of-plane piezoelectric coefficients. It is clearly seen that the Janus CrOFBr monolayer prefers the FM ground state within a biaxial strain a/a_0 range from 0.94 to 1.06. Unexpectedly, the tensile

strain can further enhance the out-of-plane piezoelectric strain coefficients d_{31} and d_{32} , which represent a 27% and 67% increase relative to the unstrained values. We believe that our study provides significant insights into the development of 2D piezoelectric materials characterized by a large vertical piezoelectric response, and it holds the potential to advance the field of nanoelectronics.

ACKNOWLEDGMENTS

This work was supported by the National Natural Science Foundation of China (No. 22372142), the Innovation Capability Improvement Project of Hebei province (No. 22567605H), the Natural Science Foundation of Hebei Province of China (No. B2021203030), and the Science and Technology Project of Hebei Education Department (No. JZX2023020). The numerical calculations in this paper have been done on the supercomputing system in the High Performance Computing Center of Yanshan University.

-
- [1] K. S. Novoselov, A. K. Geim, S. V. Morozov, D. Jiang, Y. Zhang, S. V. Dubonos, I. V. Grigorieva, and A. A. Firsov, Electric field effect in atomically thin carbon films, *Science* **306**, 666 (2004).
- [2] S. Das Sarma, S. Adam, E. H. Hwang, and E. Rossi, Electronic transport in two-dimensional graphene, *Rev. Mod. Phys.* **83**, 407 (2011).
- [3] K. S. Novoselov, A. K. Geim, S. V. Morozov, D. Jiang, M. I. Katsnelson, I. V. Grigorieva, S. V. Dubonos, and A. A. Firsov, Two-dimensional gas of massless Dirac fermions in graphene, *Nature (London)* **438**, 197 (2005).
- [4] E. H. Hwang, S. Adam, and S. D. Sarma, Carrier transport in two-dimensional graphene layers, *Phys. Rev. Lett.* **98**, 186806 (2007).
- [5] C. Gong, L. Li, Z. Li, H. Ji, A. Stern, Y. Xia, T. Cao, W. Bao, C. Wang, Y. Wang, Z. Q. Qiu, R. J. Cava, S. G. Louie, J. Xia, and X. Zhang, Discovery of intrinsic ferromagnetism in two-dimensional van der Waals crystals, *Nature (London)* **546**, 265 (2017).
- [6] B. Huang, G. Clark, E. Navarro-Moratalla, D. R. Klein, R. Cheng, K. L. Seyler, D. Zhong, E. Schmidgall, M. A. McGuire, D. H. Cobden, W. Yao, D. Xiao, P. Jarillo-Herrero, and X. Xu, Layer-dependent ferromagnetism in a van der Waals crystal down to the monolayer limit, *Nature (London)* **546**, 270 (2017).
- [7] S. D. Guo, W. Q. Mu, X. B. Xiao, and B. G. Liu, Intrinsic room-temperature piezoelectric quantum anomalous Hall insulator in Janus monolayer Fe_2IX ($X = Cl$ and Br), *Nanoscale* **13**, 12956 (2021).
- [8] X. Kong, L. Li, L. Liang, F. M. Peeters, and X. J. Liu, The magnetic, electronic, and light-induced topological properties in two-dimensional hexagonal FeX_2 ($X=Cl, Br, I$) monolayers, *Appl. Phys. Lett.* **116**, 192404 (2020).
- [9] S. D. Guo, W. Q. Mu, J. H. Wang, Y. X. Yang, B. Wang, and Y. S. Ang, Strain effects on the topological and valley properties of the Janus monolayer $VSiGeN_4$, *Phys. Rev. B* **106**, 064416 (2022).
- [10] J. Tian, J. Li, H. Liu, Y. Li, and J. Shi, Two-dimensional Janus $1T-CrXY$ ($X=S, Se, Te, Y=F, Cl, Br, I$): Multifunctional ferromagnetic semiconductor with large valley and piezoelectric polarizations, *Phys. Rev. B* **109**, 125413 (2024).
- [11] S. D. Guo, Y. L. Tao, H. T. Guo, Z. Y. Zhao, B. Wang, G. Wang, and X. Wang, Possible electronic state quasi-half-valley metal in a VGe_2P_4 monolayer, *Phys. Rev. B* **107**, 054414 (2023).
- [12] S. Kang, S. Kim, S. Jeon, W. S. Jang, D. Seol, Y. M. Kim, J. Lee, H. Yang, and Y. Kim, Atomic-scale symmetry breaking for out-of-plane piezoelectricity in two-dimensional transition metal dichalcogenides, *Nano Energy* **58**, 57 (2019).
- [13] F. Nejati, S. Fazeli, and H. Einollahzadeh, Investigation of phase transition and the effect of stress on piezoelectric coefficients in three 2D structures of In_2Se_3 , *Solid State Commun.* **348–349**, 114733 (2022).
- [14] S. D. Guo, W. Q. Mu, X. B. Xiao, and B. G. Liu, Generalization of piezoelectric quantum anomalous Hall insulator based on monolayer Fe_2I_2 : a first-principles study, *Phys. Chem. Chem. Phys.* **23**, 25994 (2021).
- [15] J. Qiu, X. Chen, F. Zhang, B. Zhu, H. Guo, X. Liu, J. Yu, and J. Bao, Highly adjustable piezoelectric properties in two-dimensional $LiAlTe_2$ by strain and stacking, *Nanotechnology* **33**, 055702 (2022).
- [16] S. E. Park and T. R. Shroud, Ultrahigh strain and piezoelectric behavior in relaxor based ferroelectric single crystals, *J. Appl. Phys.* **82**, 1804 (1997).
- [17] Y. Guo, S. Zhou, Y. Bai, and J. Zhao, Enhanced piezoelectric effect in Janus group-III chalcogenide monolayers, *Appl. Phys. Lett.* **110**, 163102 (2017).
- [18] R. Fei, W. Li, J. Li, and L. Yang, Giant piezoelectricity of monolayer group IV monochalcogenides: $SnSe, SnS, GeSe,$ and GeS , *Appl. Phys. Lett.* **107**, 173104 (2015).
- [19] L. Dong, J. Lou, and V. B. Shenoy, Large in-plane and vertical piezoelectricity in Janus transition metal dichalcogenides, *ACS Nano* **11**, 8242 (2017).
- [20] W. Wu, L. Wang, Y. Li, F. Zhang, L. Lin, S. Niu, D. Chenet, X. Zhang, Y. Hao, T. F. Heinz, J. Hone, and Z. L. Wang,

- Piezoelectricity of single-atomic-layer MoS₂ for energy conversion and piezotronics, *Nature (London)* **514**, 470 (2014).
- [21] J. Yang, A. Wang, S. Zhang, J. Liu, Z. Zhong, and L. Chen, Co-existence of piezoelectricity and magnetism in two-dimensional vanadium dichalcogenides, *Phys. Chem. Chem. Phys.* **21**, 132 (2019).
- [22] A. Kaur, S. Sharma, P. Nandi, and A. De Sarkar, Correlation between strain tunable piezoelectricity and Rashba effect in flexible Janus Ga₂Ge₂XY (X, Y = S, Se, and Te) monolayers with high carrier mobility, *Physica E* **154**, 115791 (2023).
- [23] N. Ghobadi, S. G. Rudi, and S. Soleimani-Amiri, Electronic, spintronic, and piezoelectric properties of new Janus ZnAXY (A = Si, Ge, Sn, and X, Y = S, Se, Te) monolayers, *Phys. Rev. B* **107**, 075443 (2023).
- [24] N. Tripathy and A. D. Sarkar, Anisotropy in colossal piezoelectricity, giant Rashba effect and ultrahigh carrier mobility in Janus structures of quintuple Bi₂X₃ (X = S, Se) monolayers, *J. Phys.: Condens. Matter* **35**, 335301 (2023).
- [25] T. V. Vu, H. V. Phuc, L. C. Nhan, A. I. Kartamyshev, and N. N. Hieu, Predicted novel Janus γ -Ge₂XY (X/Y = S, Se, Te) monolayers with mexican-hat dispersions and high carrier mobilities, *J. Phys. D* **56**, 135302 (2023).
- [26] D. Bezzerga, E.-A. Haidar, C. Stampfl, A. Mir, and M. Sahnoun, Ferro-piezoelectricity in emerging Janus monolayer BMX₂ (M = Ga, In and X = S, Se): *ab initio* investigations, *Nanoscale Adv.* **5**, 1425 (2023).
- [27] M. Milivojević, M. Orozovi, S. Picozzi, M. Gmitra, and S. Stavri, Interplay of altermagnetism and weak ferromagnetism in two-dimensional RuF₄, *2D Mater.* **11**, 035025 (2024).
- [28] J. Söderquist and T. Olsen, Two-dimensional altermagnets from high throughput computational screening: Symmetry requirements, chiral magnons, and spin-orbit effects, *Appl. Phys. Lett.* **124**, 182409 (2024).
- [29] S.-D. Guo and Y. S. Ang, Spontaneous spin splitting in electric potential difference antiferromagnetism, *Phys. Rev. B* **108**, L180403 (2023).
- [30] Y. Zhu, T. Chen, Y. Li, L. Qiao, X. Ma, C. Liu, T. Hu, H. Gao, and W. Ren, Multipiezo effect in altermagnetic V₂SeTeO monolayer, *Nano Lett.* **24**, 472 (2024).
- [31] S.-D. Guo, X.-S. Guo, K. Cheng, K. Wang, and Y. S. Ang, Piezoelectric altermagnetism and spin-valley polarization in Janus monolayer Cr₂SO, *Appl. Phys. Lett.* **123**, 082401 (2023).
- [32] Z.-Y. Chen, Y.-Y. Wang, T.-P. Hou, N.-S. Liu, and H.-F. Lin, Bipolar ferromagnetic semiconductors and dipole-modulated magnetism in two-dimensional Janus transition metal dihalides, *J. Appl. Phys.* **134**, 123903 (2023).
- [33] Z. Guan, N. Luo, S. Ni, and S. Hu, Tunable electronic and magnetic properties of monolayer and bilayer Janus Cr₂Cl₃I₃: A first-principles study, *Mater. Adv.* **1**, 244 (2020).
- [34] Y. Chen, Q. Fan, Y. Liu, and G. Yao, Electrically tunable magnetism and unique intralayer charge transfer in Janus monolayer MnSSe for spintronics applications, *Phys. Rev. B* **105**, 195410 (2022).
- [35] J. Zhang, S. Jia, I. Kholmanov, L. Dong, D. Er, W. Chen, H. Guo, Z. Jin, V. B. Shenoy, L. Shi, and J. Lou, Janus monolayer transition-metal dichalcogenides, *ACS Nano* **11**, 8192 (2017).
- [36] N. Jena, Dimple, S. D. Behere, and A. De Sarkar, Strain-induced optimization of nanoelectromechanical energy harvesting and nanopiezotronic response in a MoS₂ monolayer nanosheet, *J. Phys. Chem. C* **121**, 9181 (2017).
- [37] Dimple, N. Jena, A. Rawat, R. Ahammed, M. K. Mohanta, and A. De Sarkar, Emergence of high piezoelectricity along with robust electron mobility in Janus structures in semiconducting group IVB dichalcogenide monolayers, *J. Mater. Chem. A* **6**, 24885 (2018).
- [38] P. Hohenberg and W. Kohn, Inhomogeneous electron gas, *Phys. Rev.* **136**, B864 (1964).
- [39] W. Kohn and L. J. Sham, Self-consistent equations including exchange and correlation effects, *Phys. Rev.* **140**, A1133 (1965).
- [40] G. Kresse, *Ab initio* molecular dynamics for liquid metals, *J. Non-Cryst. Solids* **192–193**, 222 (1995).
- [41] G. Kresse and J. Furthmüller, Efficiency of *ab-initio* total energy calculations for metals and semiconductors using a plane-wave basis set, *Comput. Mater. Sci.* **6**, 15 (1996).
- [42] G. Kresse and D. Joubert, From ultrasoft pseudopotentials to the projector augmented-wave method, *Phys. Rev. B* **59**, 1758 (1999).
- [43] J. P. Perdew, K. Burke, and M. Ernzerhof, Generalized gradient approximation made simple, *Phys. Rev. Lett.* **77**, 3865 (1996).
- [44] V. I. Anisimov, I. V. Solovyev, M. A. Korotin, M. T. Czyżyk, and G. A. Sawatzky, Density-functional theory and NiO photoemission spectra, *Phys. Rev. B* **48**, 16929 (1993).
- [45] V. I. Anisimov, J. Zaanen, and O. K. Andersen, Band theory and Mott insulators: Hubbard U instead of stoner I, *Phys. Rev. B* **44**, 943 (1991).
- [46] N. Miao, B. Xu, L. Zhu, J. Zhou, and Z. Sun, 2D intrinsic ferromagnets from van der Waals antiferromagnets, *J. Am. Chem. Soc.* **140**, 2417 (2018).
- [47] A. K. Nair, S. Rani, M. V. Kamalakar, and S. J. Ray, Bi-stimuli assisted engineering and control of magnetic phase in monolayer CrOCl, *Phys. Chem. Chem. Phys.* **22**, 12806 (2020).
- [48] S. Baroni, S. de Gironcoli, A. Dal Corso, and P. Giannozzi, Phonons and related crystal properties from density-functional perturbation theory, *Rev. Mod. Phys.* **73**, 515 (2001).
- [49] G. J. Martyna, M. L. Klein, and M. Tuckerman, Nosé-Hoover chains: The canonical ensemble via continuous dynamics, *J. Chem. Phys.* **97**, 2635 (1992).
- [50] A. Togo, F. Oba, and I. Tanaka, First-principles calculations of the ferroelastic transition between rutile-type and CaCl₂-type SiO₂ at high pressures, *Phys. Rev. B* **78**, 134106 (2008).
- [51] C. Xu, J. Zhang, Z. Guo, S. Zhang, X. Yuan, and L. Wang, A first-principles study on the electronic property and magnetic anisotropy of ferromagnetic CrOF and CrOCl monolayers, *J. Phys.: Condens. Matter* **33**, 195804 (2021).
- [52] See Supplemental Material at <http://link.aps.org/supplemental/10.1103/PhysRevB.110.064430> for the description of negative crystal orbital Hamilton population, phonon spectrum, the energy of different magnetic configurations, energy band structures, the F-*p* orbital-resolved MAE, the planar averaged electrostatic potential energy variation along the *z* direction, out-of-plane piezoelectric strain coefficient as a function of the electronegativity difference ratio, energy band structures with *a/a*₀ changing, piezoelectric strain coefficients as a function of *a/a*₀, out-of-plane piezoelectric coefficients and magnetic moment of Cr atom as a function of *a/a*₀.

- [53] E. Cadelano and L. Colombo, Effect of hydrogen coverage on the Young's modulus of graphene, *Phys. Rev. B* **85**, 245434 (2012)
- [54] E. Cadelano, P. L. Palla, S. Giordano, and L. Colombo, Elastic properties of hydrogenated graphene, *Phys. Rev. B* **82**, 235414 (2010)
- [55] M. N. Blonsky, H. L. Zhuang, A. K. Singh, and R. G. Hennig, *Ab initio* prediction of piezoelectricity in two-dimensional materials, *ACS Nano* **9**, 9885 (2015).
- [56] Y. Chen, J. Y. Liu, J. B. Yu, Y. G. Guo, and Q. Sun, Symmetry-breaking induced large piezoelectricity in Janus tellurene materials, *Phys. Chem. Chem. Phys.* **21**, 1207 (2019).
- [57] S. D. Guo, Y. T. Zhu, W. Q. Mu, and W. C. Ren, Intrinsic piezoelectricity in monolayer MSi_2N_4 ($M = \text{Mo}, \text{W}, \text{Cr}, \text{Ti}, \text{Zr}$ and Hf), *Europhys. Lett.* **132**, 57002 (2020).
- [58] S. D. Guo, Y. T. Zhu, W. Q. Mu, L. Wang, and X. Q. Chen, Structure effect on intrinsic piezoelectricity in septuple-atomic-layer MSi_2N_4 ($M = \text{Mo}$ and W), *Comput. Mater. Sci.* **188**, 110223 (2021).
- [59] W. B. Li and J. Li, Piezoelectricity in two-dimensional group-III monochalcogenides, *Nano Res.* **8**, 3796 (2015).
- [60] S. D. Guo, X. S. Guo, Z. Y. Liu, and Y. N. Quan, Large piezoelectric coefficients combined with high electron mobilities in Janus monolayer XTel ($X = \text{Sb}$ and Bi): A first-principles study, *J. Appl. Phys.* **127**, 064302 (2020).
- [61] J. Tan, Y. H. Wang, Z. T. Wang, X. J. He, Y. L. Liu, B. Wanga, M. I. Katsnelson, and S. J. Yuan, Large out-of-plane piezoelectricity of oxygen functionalized MXenes for ultrathin piezoelectric cantilevers and diaphragms, *Nano Energy* **65**, 104058 (2019).
- [62] Y.-Q. Li, X.-Y. Wang, S.-Y. Zhu, D.-S. Tang, Q.-W. He, and X.-C. Wang, Active asymmetric electron-transfer effect on the enhanced piezoelectricity in MoTO ($T = \text{S}, \text{Se}, \text{or Te}$) monolayers and bilayers, *J. Phys. Chem. Lett.* **13**, 9654 (2022).
- [63] T. Zhang, Y. Liang, H. Guo, H. Fan, and X. Tian, The high piezoelectricity, flexibility and electronic properties of new Janus ZnXY_2 ($X = \text{Ge}, \text{Sn}, \text{Si}$ and $Y = \text{S}, \text{Se}, \text{Te}$) monolayers: A first-principles research, *Appl. Surf. Sci.* **579**, 152017 (2022).
- [64] H.-N. Zhang, Y. Wu, C. Yang, L.-H. Zhu, and X.-C. Wang, Enhanced out-of-plane piezoelectricity of group-III (A) Janus hydrofluoride monolayers, *Phys. Rev. B* **104**, 235437 (2021).
- [65] S. D. Guo, W. Q. Mu, and Y. T. Zhu, Biaxial strain enhanced piezoelectric properties in monolayer $\text{g-C}_3\text{N}_4$, *J. Phys. Chem. Solids* **151**, 109896 (2021).